Available online at www.sciencedirect.com
ScienceDirect
International Journal of Multiphase Flow 34 (2008) 1161–1174
International Journal of Multiphase Flow
www.elsevier.com/locate/ijmulflow

Experimental analysis of flow regimes and pressure drop reduction in oil–water mixtures

G. Sotgia [a], P. Tartarini [b], E. Stalio [b,*]

[a] Dipartimento di Energia, Politecnico di Milano, Italy
[b] Dipartimento di Ingegneria Meccanica e Civile, Università degli Studi di Modena e Reggio Emilia, Via Vignolese 905/B, 41100 Modena, Italy

Received 20 December 2007; received in revised form 29 May 2008; accepted 1 June 2008
Available online 17 June 2008

Abstract

The physical understanding of two-phase flow characteristics in horizontal pipes is of importance in the petroleum industry since significant savings in pumping power can be derived from the water-lubricated transportation of crude oil.

An experimental study of water continuous oil–water flow in horizontal pipes is performed using mineral oil and tap water of viscosity ratio about 900 and density ratio 0.9. A set of seven different pipes of Pyrex and Plexiglas where used, with diameters ranging between 21 and 40 mm. Pressure drop measurements, flow pattern maps and clear pictures of the oil–water flow are reported in this article together with comprehensive comments. The results obtained are compared to empirical laws, theoretical findings and experimental results by different authors in the literature.

In order to identify the regions with operational conditions that are suitable for applications, a novel criterion for the location of the annular/stratified transition is proposed which is based only on experimental observations.

Keywords: Oil–water; Annular; Stratified; Transitional boundary; Pressure drop reduction

1. Introduction

The widespread occurrence of multiphase flows in pipes has motivated extensive research in the field; a number of practical applications in the petroleum industry involve oil–water two-phase flow phenomena. Significant savings in the pumping power required for oil transportation can be attained when water flows in the pipeline together with the oil, especially when the highly viscous phase is surrounded by a water annulus, giving place to the core annular flow configuration. As the establishment of a particular flow regime depends upon the interaction of gravitational, inertial and surface tension forces, annular flow is observed only under particular combinations of the oil and water flow rates.

A large body of literature is presently available on the two-phase flow of oil and water in pipes. A thorough report of industrial applications and annular flow studies made before 1997 is provided in the review by Joseph et al. (1997). The same group published a book on the topic (Joseph and Renardy, 1993) and a number of papers ranging from the linear stability analysis for the pipe flow of two liquids (Joseph et al., 1984) to an experimental study including results from a 0.6-m diameter, 1000-m-long pipeline (Joesph et al., 1999). Measurements of pressure drop and holdup for water lubricated transportation of oil in a 15.9 mm glass pipeline are presented by Arney et al. (1993) together with a friction factor formula based on concentric cylindrical core annular flow theory and an empirical equation for the holdup volume fraction.

Ooms and co-workers analyzed the case of a wavy, eccentric core annular flow with a rigid core and a thin annulus; they interpreted the balancing of buoyancy with laminar (Ooms, 1972; Ooms and Beckers, 1972; Oliemans

* Corresponding author. Tel.: +39 059 2056144; fax: +39 059 2056126.
E-mail addresses: giorgio.sotgia@polimi.it (G. Sotgia), tartarini.paolo@unimore.it (P. Tartarini), enrico.stalio@unimore.it (E. Stalio).

0301-9322/$ - see front matter © 2008 Elsevier Ltd. All rights reserved.
doi:10.1016/j.ijmultiphaseflow.2008.06.001

and Ooms, 1986; Ooms and Poesio, 2003) and turbulent (Oliemans et al., 1987) hydrodynamic lifting. The theory requires the knowledge of the wavy interface shape and is not easily applied for practical purposes. A two-fluid model which is instead commonly used to predict pressure gradient and holdup in liquid–liquid annular flows was devised by Brauner (1991). The following year Brauner and Maron (1992a) proposed a set of criteria for the transition between stratified, annular and dispersed flow patterns and tackled (1992b) the stability of stratified liquid–liquid flow. Recently Brauner developed a model for the dispersed flow regime (2001).

Angeli and Hewitt (1998) performed measurements on the flow of a low viscosity oil and tap water in two 25.4-mm pipes of stainless steel and acrylic resin; they noticed a large difference between pressure gradients measured in the two pipes and ascribed the effect to different wettability characteristics of the pipe walls. Also flow patterns were found to be substantially dependent on the pipe material, the flow structure being investigated through video recording and the use of a high frequency impedance probe (Angeli and Hewitt, 2000). The flow pattern maps provided by Angeli and Hewitt (2000) and Lovick and Angeli (2004) and the transition criteria introduced by Brauner and Maron (1992a) are compared by Chakrabarti et al. (2007) to their own map. This was compiled using quantitative indications coming from a newly designed, non-intrusive optical probe in a 25.4-mm Perspex pipe. The comparisons between maps in the papers by Angeli and Hewitt (2000) and Chakrabarti et al. (2007) reveal a marked sensitivity of liquid–liquid flow results to the many experimental parameters.

When annular flow is used for the lubricated transportation of a highly viscous oil, the liquid–liquid system is more conveniently operated far from the transition boundary with the stratified flow. The reasons are twofold, first the pressure drop reduction is larger for higher oil flow rates and second, the undesired occurrence of the transition to the stratified configuration would lead to a sharp increase in the pressure drop. The accurate and reliable prediction of the transitional boundaries between annular flow and the stratified configuration is therefore of recognized importance for applications. Bannwart (2001) reports two necessary requirements for the occurrence of annular flow. The first comes from the paper by Joseph et al. (1984) but was derived under very specific conditions for density-matched liquids, the other was suggested by the Eötvös number classification of liquid–liquid systems but fails even to follow the trends observed experimentally. On the other hand the equations for the identification of annular/stratified transitional boundaries provided by Brauner and Maron (1992b) are not straightforward to use for engineering applications because only implicitly defined functions are provided. Moreover while the holdup ratio of the flow is needed to perform the required calculations, the holdup itself depends on the flow pattern.

This paper presents an experimental study of water continuous oil–water flows; the oil used in the experiments is very viscous, with properties similar to crude oil transported in industrial pipelines. The liquid–liquid pressure drop behavior is related to the superficial velocities of the two phases and their configuration; results are compared with empirical and theoretical models in the literature. Discussion is made of the influence on the two-phase flow features of the inlet mixer, the pipe material and its history; flow pattern maps are compiled for two different pipe diameters displaying results from a large number of experiments, together with clear pictures of the wide variety of flow configurations. A criterion for the location of boundaries between annular and stratified flow is provided. In contrast with other criteria for the annular/stratified transition (Joseph et al., 1984, 1992b, 2001), the condition presented here arises only from experimental observation and does not include indications for the transition of different fluids over a very wide range of diameters. However the use of the suggested condition in applications is viable, requiring only a preliminary test to be performed using the same fluids. This would ensure an accurate indication of the most suitable flow parameters for lubricated transportation of highly viscous liquids over a wide range of conditions.

2. Experimental apparatus

The experiments reported in this paper were performed in the two-phase thermo-fluid dynamics laboratory of the *Politecnico di Milano*, in the liquid–liquid flow facility shown schematically in Fig. 1.

2.1. Description of the test facility

Oil and water are pumped separately from their storage tanks; in transit to the test section their flow rates are mea-

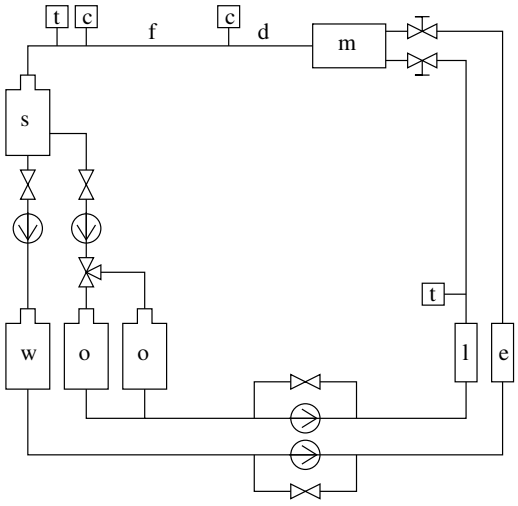

Fig. 1. Schematic representation of the oil–water loop, (o) oil Reservoir, (w) water reservoir, (l) laminar flowmeter, (e) electromagnetic flow meter, (t) thermocouple, (m) two-phase mixer, (d) flow development region, (f) fully developed flow, (c) capacitance pressure transducer, (s) separator tank.

sured by a magnetic flowmeter for the water and a laminar flowmeter for the oil. The two liquids are introduced into the test section through a coaxial mixer, shown in Fig. 2, which is designed to let the oil flow about the pipe axis while the water is injected through an annulus into the oil stream. The test rig is designed to accommodate pipes of different diameters. Pipes of Pyrex and Plexiglas are used instead of the metal pipes found in the applications, because of their advantage in being transparent.

In the test section, the pressure gradient is measured by a differential pressure transducer over the last four meters of the pipe, the full pipe length is 10 m and the flow is free to develop over a 6-m length, equivalent to 200 diameters for a $D = 30$ mm pipe and 150 diameters for $D = 40$ mm. At a distance 8 m from the inlet, visualization of the flow by video or photographic means is permitted through a visualization section. It includes a transparent box filled with water to reduce optical distortion caused by refraction. After the test section, the mixture flows to a separator tank where gravitational separation of the two liquids is obtained in about 30 min. The two fluids are then returned to their storage tanks before they can be recirculated.

2.2. Instrumentation

The experimental set-up is equipped with instrumentation for measuring and controlling the mass flow rates of the two fluids prior to mixing and the pressure drop of the two-phase flow. The instrumentation installed along the test section is listed below:

- A K-type Chromel/Alumel thermocouple (TERSID, Italy) is used to measure the temperature in the oil feed line. The temperature value is employed to account for the variation of viscosity in the measurement of the oil flow rate.
- The laminar flowmeter for the oil consists of two pressure tappings 250 mm apart connected to a SETRA differential capacitance pressure transducer having an accuracy of ±0.17% of the measured value, and a full scale of 172 kPa. The flowmeter is calibrated regularly by the "weighing method", *i.e.* weighing the fluid discharged during a measured time interval. Owing to the influence of fluid viscosity changes, measurements are corrected for temperature variations.
- The electromagnetic flow meter used for the water flow rate has a tunable range with an accuracy of 0.5% of reading (ENDRESS + HAUSER Promag F, Switzerland).
- The pressure gradient of the two-phase flow is evaluated by a differential capacitance SETRA pressure transducer. The accuracy of the device is ±0.27% of reading, confirmed with regular calibration checks.

The signals from the differential pressure transducers and the thermocouples are recorded in the hard disk of a computer equipped with a data acquisition card.

3. Experimental work

3.1. Governing parameters

The *superficial velocity* J (m/s) is defined as the ratio between the volumetric flow rate of one single phase and the pipe section

$$J_o \equiv \frac{\dot{V}_o}{S}; \qquad J_w \equiv \frac{\dot{V}_w}{S} \tag{1}$$

the *mixture superficial velocity* equals the average velocity of the mixture, $J_{ow} \equiv J_o + J_w$.

In order to assess the pumping power economy relative to the single phase flow of oil, a *pressure drop reduction factor*, is defined as

$$R \equiv \frac{\Delta p_o}{\Delta p_{ow}} \tag{2}$$

where Δp_{ow} is the measured pressure drop of the two-fluid flow and Δp_o is the pressure drop calculated using the Hagen–Poiseuille law for the single-phase laminar flow of oil having the same flow rate as the oil phase in the two-phase case. The pressure drop reduction factor has already

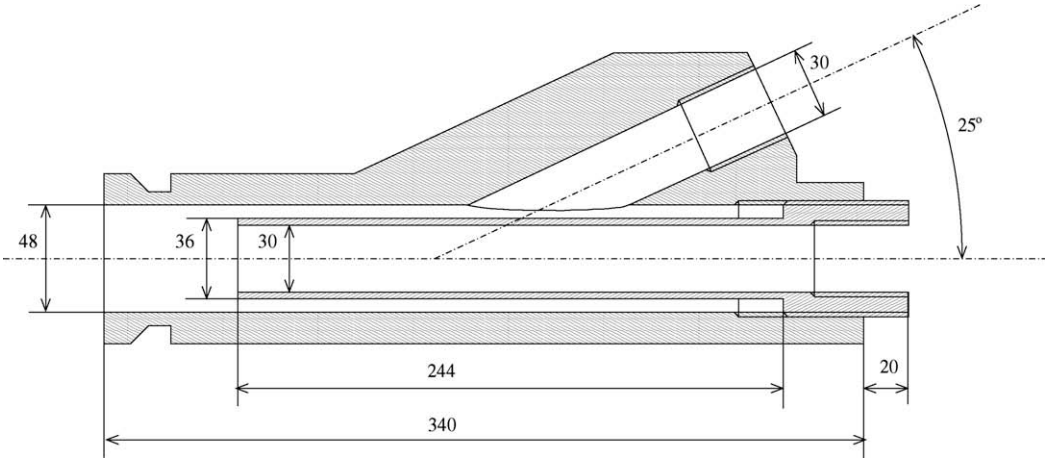

Fig. 2. Oil–water mixer. Lengths indicated on the drawing are in millimeters, angles are in degrees.

been used by a number of authors, notably Russel and Charles (1959), Oliemans and Ooms (1986) and Brauner (1991).

In the following discussion, the reduction factor is plotted against the *water input ratio* ε_w which is defined as

$$\varepsilon_w \equiv \frac{J_w}{J_{ow}} \tag{3}$$

For a fixed value of the oil superficial velocity, the maximum pressure drop reduction factor is indicated by R_{max}. The *holdup volume fraction* is defined as

$$H_w \equiv \frac{V_w}{V_o + V_w} \tag{4}$$

where V_w is the volume of water in the pipe, V_o is the volume of oil in the pipe.

The high viscosity liquid is an emulsion composed of a very small part of water in mineral oil (Milpar 220, with $\mu_o = 0.919$ Pa s and $\rho_o = 889$ kg/m^3 at 20 °C). The low-viscosity liquid is tap water, with a measured dynamic viscosity $\mu_w = 1.026 \times 10^{-3}$ Pa s and an oil content as low as 0.01%. The measured oil-water interfacial tension is $\sigma = 20 \times 10^{-3}$ N/m.

Table 1 provides a summary of the range of conditions investigated.

3.2. Experimental procedure

Experiments are performed following the procedure below:

(1) J_o is selected;
(2) the water superficial velocity span ($J_{w,min}$ and $J_{w,max}$) is selected;
(3) the experiment is started introducing only water, for $J_w > J_{w,max}$
(4) oil is introduced at the selected flow rate J_o
(5) the water flow rate is decreased to $J_{w,max}$
(6) the water superficial velocity is varied in steps between $J_{w,max}$ and $J_{w,min}$.

3.3. Flow pattern identification

Identification of flow patterns and transition boundaries is performed by visual observation through the pipe wall, supplemented by photographic and video techniques. Pictures are taken and video records made using a Canon XM2 video camera with a continuous high-intensity 800 W light source used for illumination. The pictures displayed in the present article are obtained with the light illuminating the pipe from a distance $l \approx 0.6$ m from the pipe and at an angle of about 45 °C. Shadows produced in this way reveal the three-dimensional shape of the oil–water interface.

Table 1
Summary of experimental conditions

Pipe	D (mm)	J_o (m/s)	ε_w
Plexiglas	21	0.35–0.90	0.05–0.90
	26	0.19–0.97	0.03–0.85
	30	0.25–0.87	0.04–0.85
	40	0.26–0.68	0.05–0.90
Pyrex	21.5	0.22–0.94	0.05–0.90
	28	0.27–0.92	0.05–0.90
	40	0.17–0.75	0.03–0.90

3.4. Wetting behavior of pipe surfaces

In a recent article, Santos et al. (2006) show that steel pipes are prone to wettability alteration that involves interaction between the polar oil components and the solid wall. For acrylic pipes also, Angeli and Hewitt (1998) report a slight dependence of the contact angle on the history of the solid surface; Lovick and Angeli (2004) found that for consistency in the results of their experiments it was necessary to prewet the wall with oil.

In Fig. 3 the reduction factor is plotted against the water input ratio in two initial series of experiments: the first used a brand new 28 mm Pyrex pipe and the second used the same pipe, well cleaned, but after being exposed to the oil (and the water) for a couple of days. It may be deduced from Fig. 3 that also for Pyrex pipes a significant change in the chemical and mechanical properties of the wall takes place after the exposure to the oil. Such modification proved to be permanent since after the "aging" and despite careful cleaning of the tube, pressure drop measurements then became repeatable at the modified level to better than ±5% of the measured value under most operational conditions. All results presented in the paper were obtained after exposure of the pipe wall to the oil–water mixture for some time and in fact the pressure drop measurements were repeatable within a few percent.

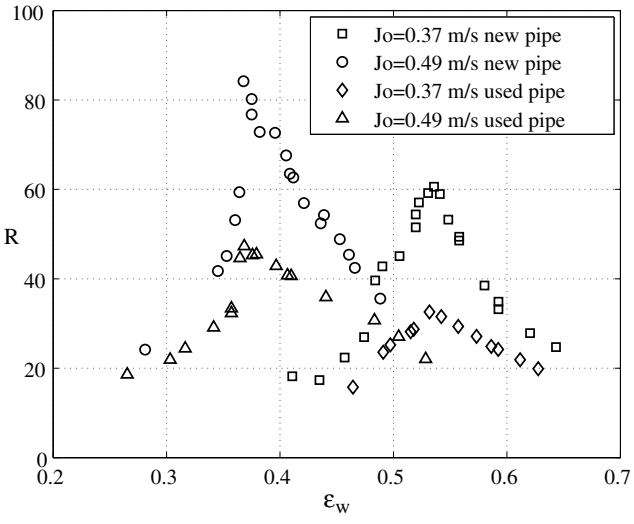

Fig. 3. Reduction factor measured for $J_o = 0.37$ and 0.49 m/s in a brand new, 28 mm Pyrex pipe and in the same pipe after being wetted by the oil.

3.5. The two-phase flow mixer

The two-phase mixer displayed in Fig. 2 was used to obtain all the experimental data presented in the following sections. The mixer had an inner diameter $D_{mixer} = 48$ mm and was fitted to the different pipes through the insertion of conical contractions made of Plexiglas.

In order to ascertain the dependence of the flow patterns and pressure drops on the method of introduction of the two phases, a preliminary set of experiments was performed. The curves displayed in Fig. 4 show a strong dependence of the measured pressure drop on different contractions used to connect the mixer to the 28-mm pipe.

The different behavior of the reduction factor, convex or concave, corresponds to different oil–water flow patterns. Visual observations reveal that for gradual contractions (C1 and C2), separate flow regimes are sustained while, when the interaction between the two phases is more strongly induced by the presence of an orifice (configuration C4), only dispersed flow patterns are observed. For configuration C4 and very low water input ratios ($\varepsilon_w < 0.1$), a previously unobserved flow pattern is recorded which is characterized by the presence of flake-shaped structures of oil around the pipe wall but not in contact with it. The presence of these "flakes" is hence associated with a relatively high reduction factor.

The contractions used in the experiments have similar characteristics as the C1 contraction of Fig. 4 and a cone angle which is always $\alpha < 15^\circ$. Results presented in this article can be considered as obtained after a smooth introduction of the two phases.

3.6. Error analysis

A detailed error analysis was carried out leading to both an estimate of the uncertainty in the measurements of the pressure drop reduction factor and the assessment of their reproducibility. The estimate of uncertainty is performed using the uncertainty propagation technique, the accuracy of the measuring instruments being obtained from the technical specifications or from calibrations. Repeated measurements at the same experimental conditions led to an estimate of the reproducibility of results.

In Table 2, which gives examples of results of the error analysis, U indicates the combined standard uncertainty in the measurements of R multiplied by a coverage factor of 2, which for normally distributed data would correspond to the 95% confidence interval. The standard deviation σ is calculated from a series of 10 measurements in the same

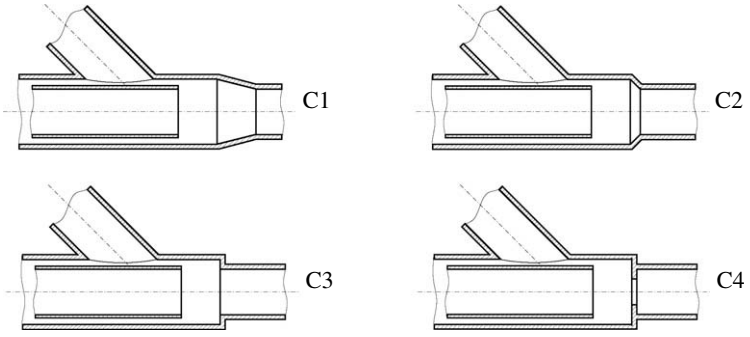

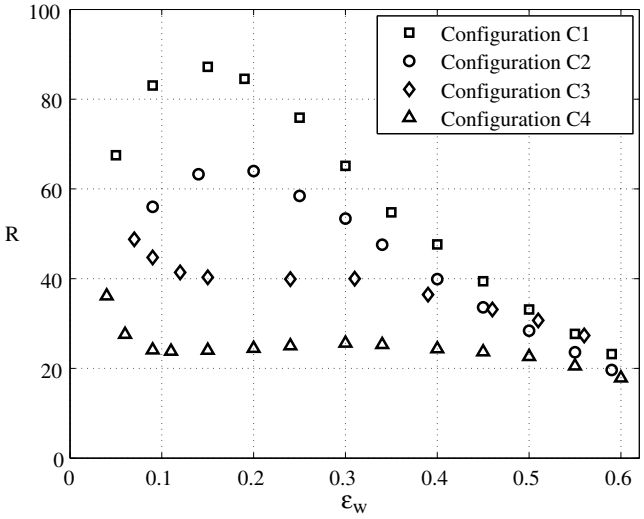

Fig. 4. Reduction factor measured using four different two-phase mixers.

conditions, and it characterizes the reproducibility of the results.

A smaller uncertainty than dispersion is noticed, moreover the dispersion depends on the operational conditions. The system exhibits a sensitive dependence on the pipe wall characteristics, the dispersion in the Plexiglas pipes being always larger than the one evaluated for Pyrex pipes. As discussed in Section 3.4, pipes used in the experiments are prone to unpredictable wettability alteration which was not accounted for in the calculation of the uncertainty. A full description of the error analysis performed is available in a conference paper by Marchesi et al. (2004).

4. Results

4.1. Flow regime observations

Figs. 5–8 display the main stages of four experimental runs that are representative of most observations. Each picture series follows the progress of flow patterns when the oil superficial velocity J_o is held constant while J_w is decreased in steps. Figs. 5 and 6, are relative to the 26-mm Plexiglas pipe. Pictures taken during experiments in the 40-mm Pyrex pipe are displayed in Figs. 7 and 8.

In Fig. 5 the evolution from dispersed to wavy stratified regime is shown for $J_o = 0.50$ m/s. When the water superficial velocity is decreased from $J_w = 2.51$ m/s the dispersed flow undergoes a long transition process (between $J_w \approx 1.9$ and 1.4 m/s) after which the oil becomes continuous in the central core, giving place to the core annular flow. Droplets of different sizes can be observed next to the fairly distorted oil–water interface, but with decreasing J_w they are perfectly absorbed by the oil core. For even lower water flow rates the annular flow evolves into a wavy annular pattern, where regular, large amplitude interfacial waves are found at the bottom of the oil core. When J_w is further decreased, the flow experiences a transition to the stratified regime after which the pipe wall is wetted also by the oil phase. In the wavy stratified regime the wavelength of the interfacial waves is smaller for decreasing J_w.

The flow pattern evolution observed in the same pipe for $J_o = 0.88$ m/s and displayed in Fig. 6 differs from the $J_o = 0.50$ m/s case mainly because in the range of water flow rate of our experiments, a stratified pattern does not appear for $J_o = 0.88$ m/s. Instead, for water superficial velocities between $J_w \approx 1.9$ and 1.4 m/s a corrugated annular configuration is observed, with fine ripple waves on the interface between the two liquids.

The flow pattern evolution displayed in Fig. 7, for $J_o = 0.48$ m/s in a $D = 40$-mm Pyrex tube displays similarities to the one described for the 26-mm Plexiglas pipe at comparable oil superficial velocity (Fig. 5), the most evident differences being the modifications of the shape of the oil core before transition to the stratified regime. Also in the 40-mm Pyrex tube, for larger oil superficial velocities, the occurrence of the stratified flow pattern is not evident. The annular, wavy annular and corrugated annular flow patterns for $J_o = 0.75$ m/s are displayed in Fig. 8.

Table 2
Uncertainties and standard deviations in the measurement of R

Pipe	D (mm)	J_o (m/s)	U/R (%)	$2\sigma/R$ (%)
Plexiglas	40	0.39	3.4	4.6
	40	0.57	3.8	8.8
	40	0.69	2.7	8.2
Pyrex	40	0.39	2.8	2.4
	40	0.57	1.8	2.2
	40	0.69	2.1	5.8

4.2. Flow pattern maps

Flow pattern maps compiled for the 26-mm Plexiglas pipe and the 40-mm Pyrex pipe are shown in Figs. 9 and 10 respectively, where the regions of existence of the various patterns are indicated. A broad buffer zone is shown between the dispersed and the core annular flow regime, this is because visual observation of such a gradual transition does not allow a sharp boundary to be discerned between the two regimes.

Fig. 9 displays also the points of the map where, for a selected oil superficial velocity, the peak reduction factor is reached. As expected, R_{max} is found next to the lower J_w boundary of the annular flow regime regions. It is noticed from Figs. 9 and 10 that for sufficiently low oil superficial velocities ($J_o < \widehat{J}_o$), when starting from a core annular flow regime while the input water rate is progressively decreased, the annular flow undergoes a transition to the stratified regime. For oil superficial velocities exceeding $\widehat{J}_o$, the stratified regime does not occur anymore and core annular, wavy annular or corrugated annular patterns are observed for a wide range of water superficial velocities. A critical value of the oil superficial velocity $\widehat{J}_o$ may be identified; beyond this the stratified regime is not sustained.

When core flows are employed for viscous oil transportation, suitable operational conditions are selected near the line of maximum reduction factor, displayed in Fig. 9. However it is well known (Arney et al., 1993) that the onset of the stratified regime is to be avoided since it involves contact of the oil with the pipe wall and a sudden drop in reduction factor. Below the critical oil superficial velocity, for conditions next to the optimal R_{max}, a slight change in the water input rate could determine an undesired transition to the stratified regime.

The value of $\widehat{J}_o$ depends in general on a number of geometrical parameters: tube diameter, roughness, contact angle, as well as the two fluids rheological properties. A critical oil superficial velocity of $\widehat{J}_o \approx 0.6$ m/s was found for the 40-mm Pyrex pipe; for all the other conditions investigated the critical superficial velocity was evaluated as $\widehat{J}_o \approx 0.7$ m/s.

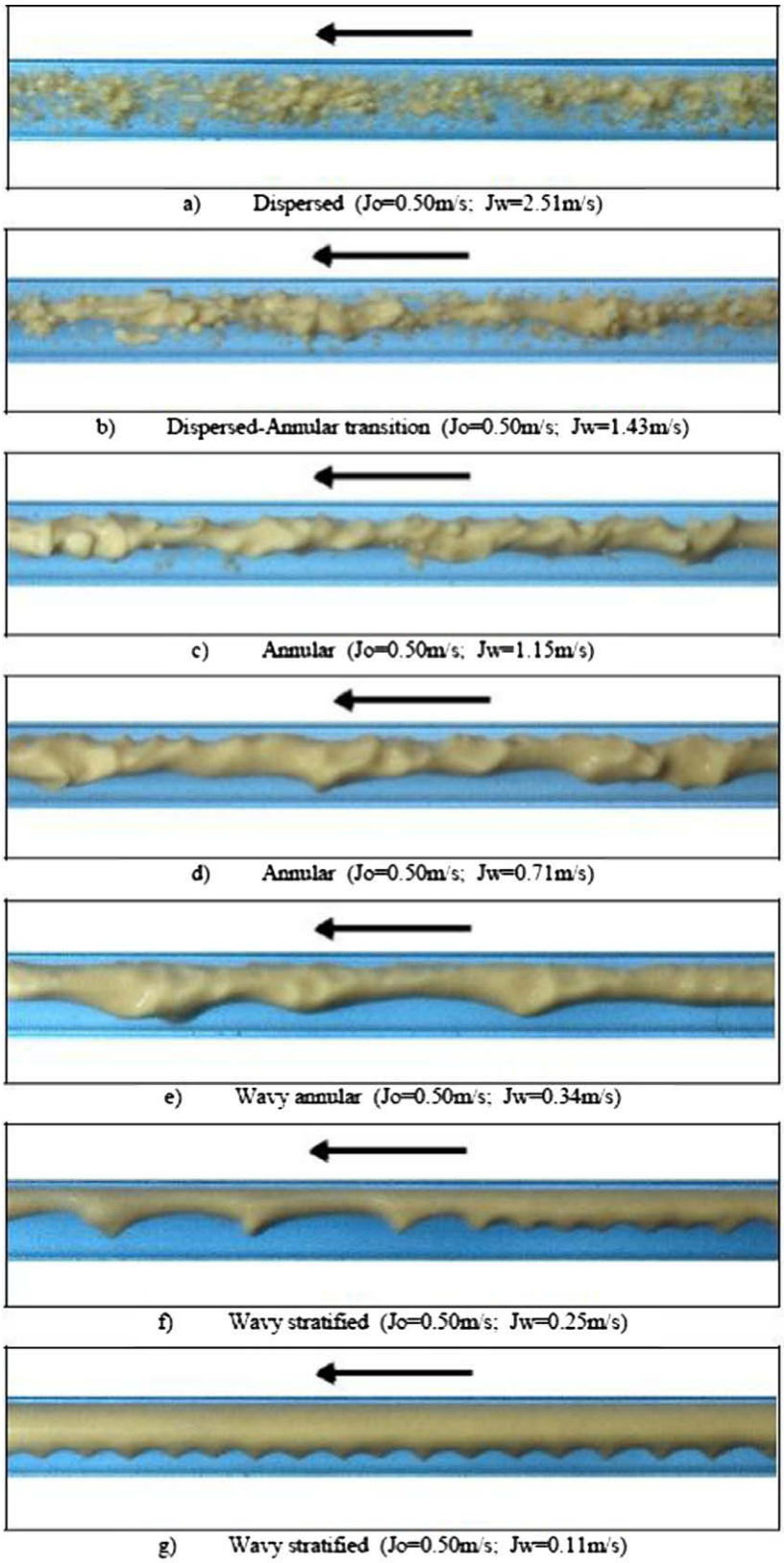

Fig. 5. Flow patterns observed for $J_o = 0.50$ m/s in the 26-mm Plexiglas tube.

4.3. Reduction factor plots

Whereas in annular flow conditions the water wets the entire pipe circumference, in the stratified pattern the pipe is wetted also by the oil and the lubricating effect of the water phase becomes less effective. As a consequence, transition of the core annular flow to the stratified regime is characterized by a pressure drop behavior which is markedly different

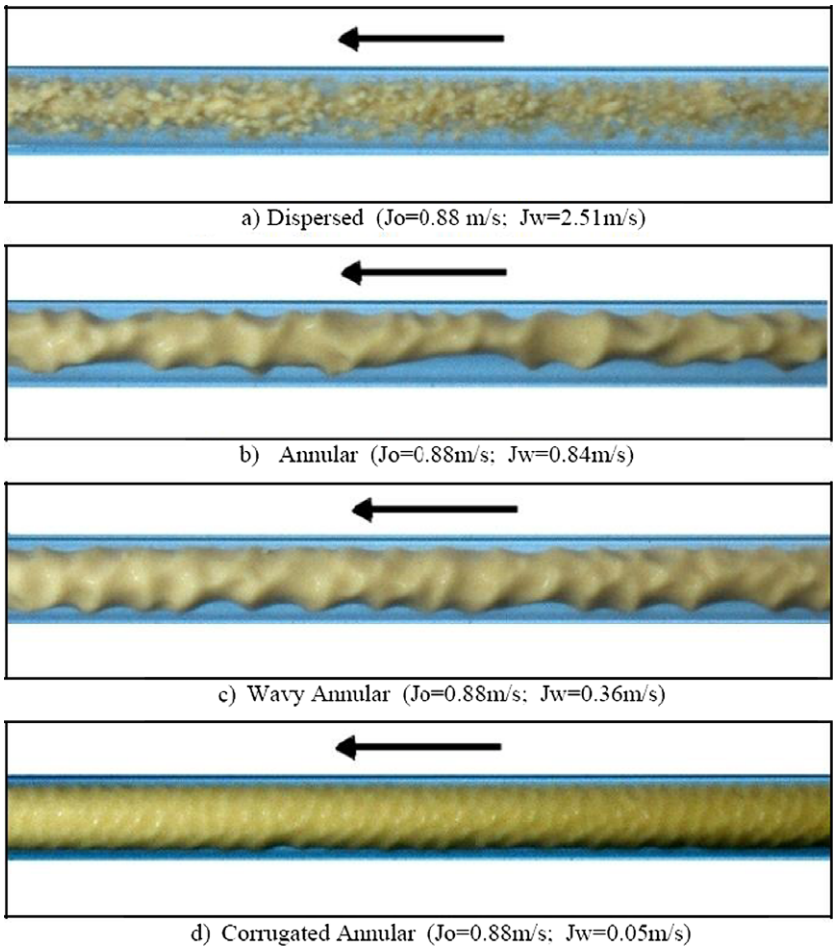

Fig. 6. Flow patterns observed for $J_o = 0.88$ m/s in the 26-mm Plexiglas tube.

from the transition that leads firstly to the wavy annular, then the corrugated annular regime. This is shown in Figs. 11 and 12 where the progress of the experiments is in the direction of the decrease of the water fraction, therefore the plots should be red from right to left.

When oil is transported in the core annular regime at a given superficial velocity $J_o < \widehat{J}_o$ and the water flow rate is progressively decreased, the pressure gradient starts decreasing with a corresponding rise in R. After the peak reduction factor is reached, the pressure gradient experiences a steep increase, resulting in a sudden drop of R, clearly visible in Fig. 11. When ε_w is decreased from the annular flow range where $J_o > \widehat{J}_o$, an increase of the reduction factor is observed until a maximum is attained, then R diminishes smoothly with no dangerous jumps in pressure drop. This behavior, displayed in Fig. 12, corresponds to the smooth modification of a corrugated annular regime.

The maximum reduction factor as a function of the oil superficial velocity is displayed in Fig. 13 for four different cases. In agreement with the results of Oliemans and Ooms (1986), R_{max} curves are shown to be lower for increasing pipe diameters. They show a maximum in the upper range of the oil superficial velocities of the experiments, and always for $J_o > \widehat{J}_o$. The most convenient flow regimes in terms of pumping power economy fall far from the transition boundary with the stratified flow.

Fig. 14 displays water input ratios $\varepsilon_{w,max}$ corresponding to reduction factor maxima over the range of diameters investigated. It is noticed that in the lower J_o range $\varepsilon_{w,max}$ is independent of the pipe diameter and material while for $J_o > 0.8$, $\varepsilon_{w,max}$ is almost constant. In the most convenient flow regimes the volumetric flow rate of the water transported in the pipe is about 10% of the mixture flow rate. This is in agreement with the result by Ullmann and Brauner (2004), where the predicted $\varepsilon_{w,max}$ ranges between 0.08 and 0.12, for turbulent flow of the water and laminar oil core.

4.4. Comparison with model predictions

In this section, experimental results are compared to a model devised by Brauner (1991) for predicting the pressure drop of two immiscible liquids in fully developed, annular flow conditions. Comparison is also made to an extension of the Blasius formula to the core annular flow case introduced by Arney et al. (1993) that successfully reduces data from different investigations to a single curve.

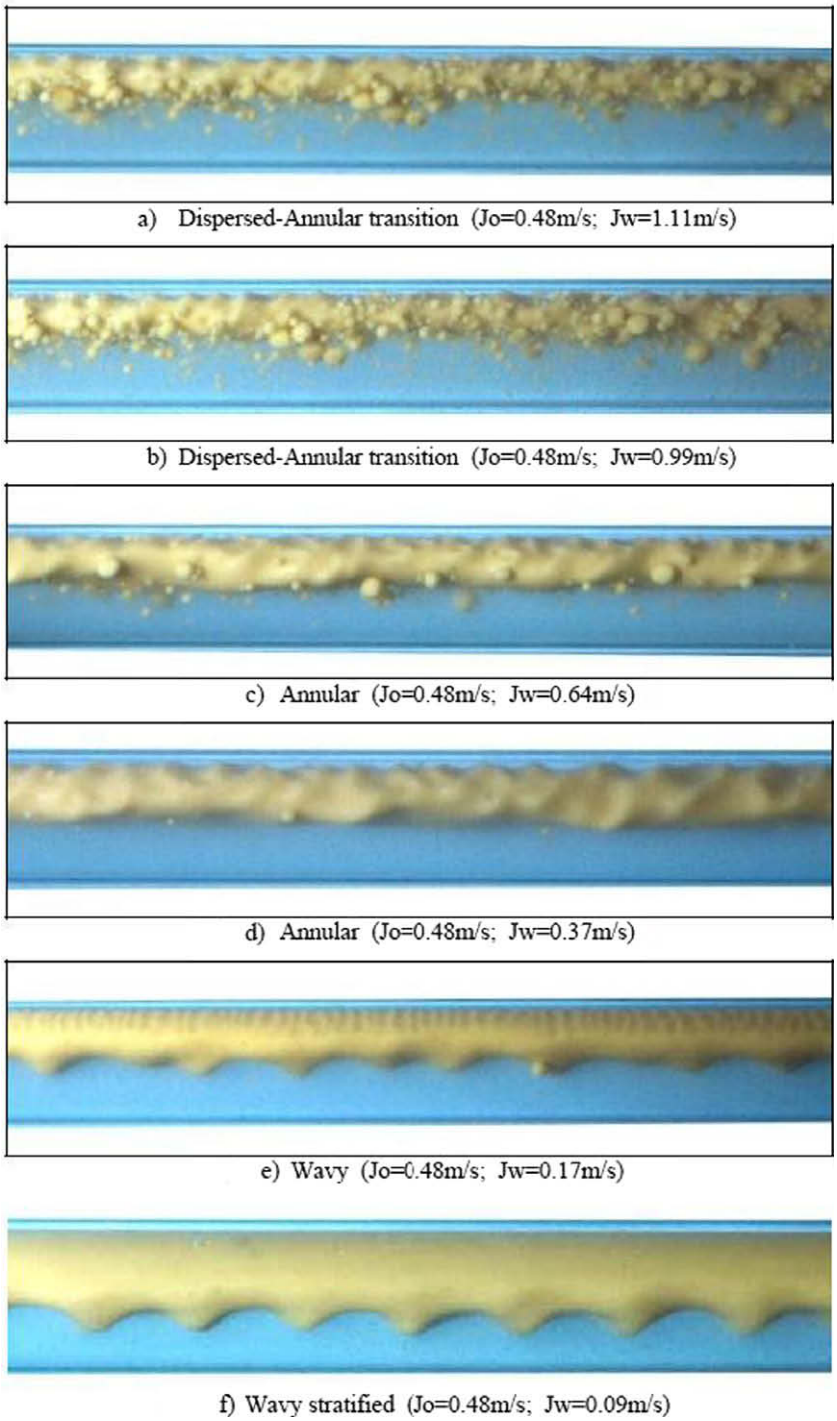

Fig. 7. Flow patterns observed for $J_o = 0.48$ m/s in the 40 mm Pyrex tube.

The correlation by Brauner is derived from the integral form of the momentum equations for the two fluids, where interfacial and wall shear stress are expressed in terms of the corresponding friction factors. It can be applied to all possible combinations of laminar or turbulent regime of the core and annular flows, the critical Reynolds number of the superficial velocities being set to $Re_s = 1500$. The two-phase pressure gradient in dimensionless form ($\Phi = 1/R$) is given by:

$$\Phi_B = \frac{K_1}{\phi}\left[\frac{(K_1\phi)^{1/2} + \phi + 1}{(K_1\phi)^{1/2} + 1}\right]^2 \tag{5}$$

where ϕ is defined as the ratio between the superficial velocities of the fluids involved ($\phi = J_o/J_w$). The coefficient K_1 for the laminar core and turbulent annular phase, which is the case for the present experiments, is given by the expression

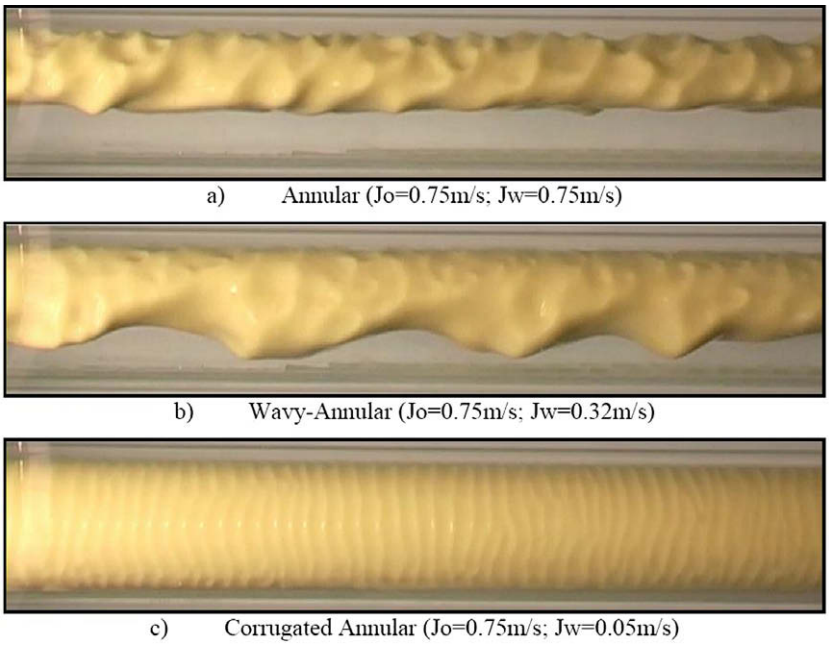

Fig. 8. Flow patterns observed for $J_o = 0.75$ m/s in the 40 mm Pyrex tube.

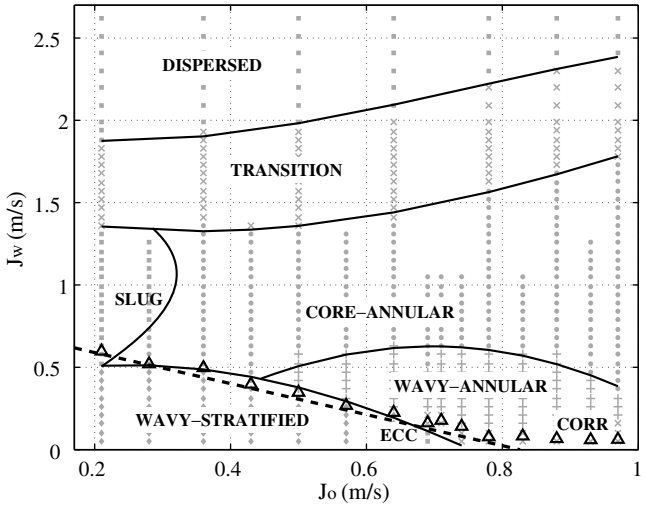

Fig. 9. Flow pattern map for the 26-mm Plexiglas pipe. Triangles indicate (J_o, J_w) values associated with R_{max}. Solid lines are third degree polynomials representing the boundaries between flow patterns. The dashed line corresponds to Eq. (18) for $\omega_t = 2.3$ m/s.

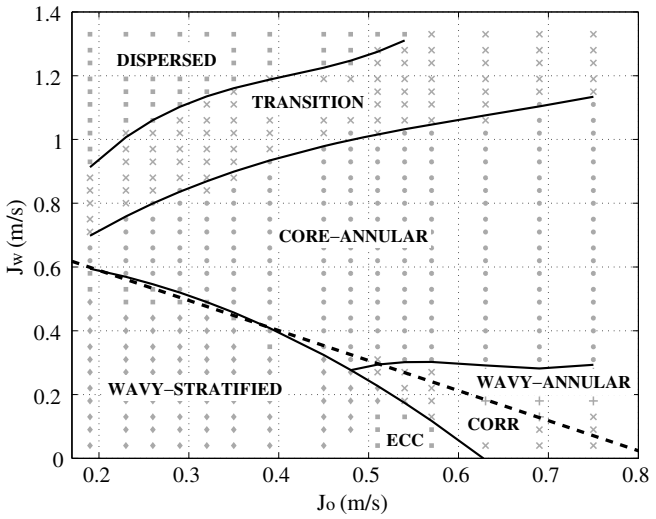

Fig. 10. Flow pattern map for the 40-mm Pyrex pipe. Solid lines are Third-degree polynomials representing the boundaries between flow patterns. The dashed line corresponds to Eq. (18) for $\omega_t = 2.3$ m/s.

$$K_1 = \frac{0.046}{16}\,\frac{\mu_w}{\mu_o}\,Re_{s,w} \tag{6}$$

The superficial Reynolds number of the water phase is defined as $Re_{s,w} \equiv \rho_w J_w D/\mu_w$ while μ_w and μ_o indicate the water and the oil viscosities.

Arney et al. (1993) developed a simple theory based on cylindrical core annular flow and yielding to the definitions of an appropriate Reynolds number and a friction factor to be substituted in the Blasius formula for predicting the two-phase pressure drop in the annular flow regime. In order to obtain a non-dimensional pressure drop Φ_A through the formulation by Arney et al. (1993), the holdup volume fraction, not measured in the present study, is first evaluated from an empirical formula provided by the same authors

$$H_w = \varepsilon_w[1 + 0.35(1 - \varepsilon_w)] \tag{7}$$

The non-dimensional core diameter $\eta = D_c/D$ can be then used to compute the *composite density* ρ_c, Eq. (9), the Arney formulation of the Reynolds number Re_A, Eq. (10), and finally the friction factor from the Blasius formula.

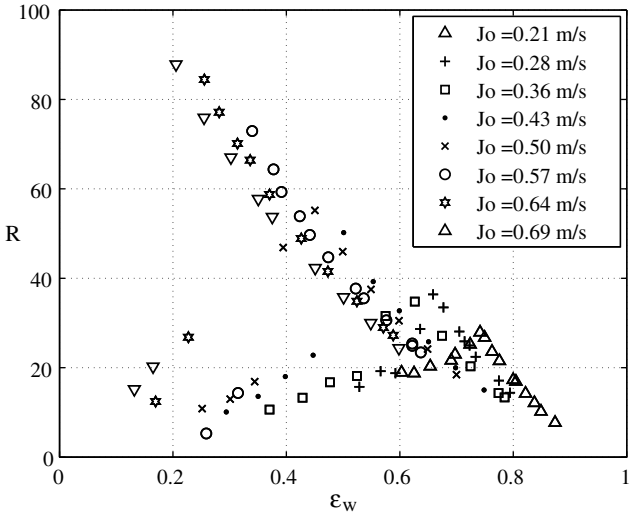

Fig. 11. Pressure drop reduction factor measured in the 26-mm Plexiglas pipe for decreasing ε_w and for different oil superficial velocities, $J_o < \widehat{J}_o$.

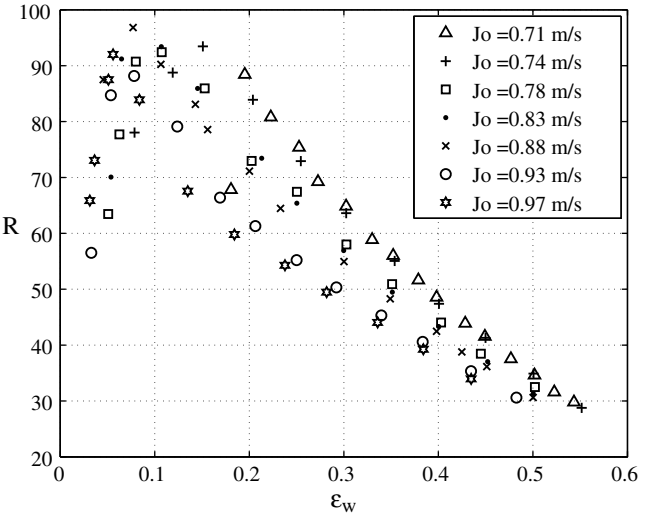

Fig. 12. Pressure drop reduction factor measured in the 26-mm Plexiglas pipe for decreasing ε_w and for different oil superficial velocities, $J_o > \widehat{J}_o$.

$$\eta = \sqrt{1 - H_w} \tag{8}$$

$$\rho_c = (1-\eta^2)\rho_w + \eta^2\rho_o \tag{9}$$

$$Re_A = \frac{\rho_c D J_{ow}}{\mu_w}\left[1 + \eta^4\left(\frac{\mu_w}{\mu_o} - 1\right)\right] \tag{10}$$

$$\lambda_A = 0.316 Re_A^{-\frac{1}{4}} \tag{11}$$

The dimensionless pressure drop is given by

$$\Phi_A = \frac{\rho_c D J_{ow}^2}{64\mu_o J_o}\ \lambda_A \tag{12}$$

Fig. 15 compares the pressure drop reduction factor evaluated through the Brauner's model, Eq. (5), the model by Arney et al. which results in Eq. (12) and the present experiments in the 26-mm Plexiglas pipe. The comparison is shown for three different oil superficial velocities.

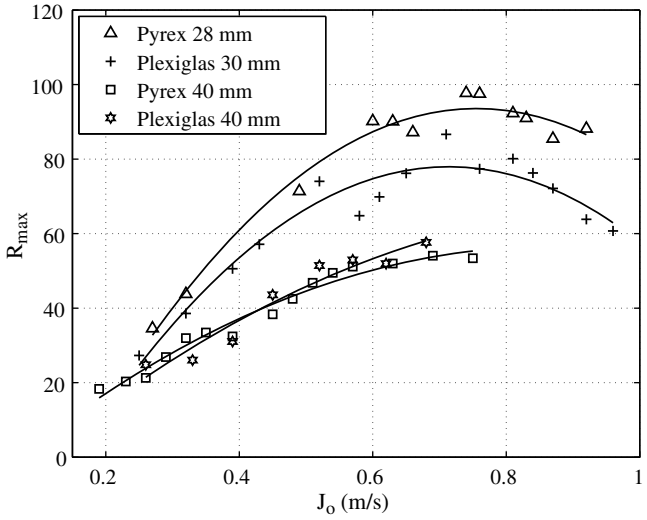

Fig. 13. Pressure drop reduction factor maxima as functions of the oil superficial velocity. Solid lines are second degree polynomials fitting the experimental data.

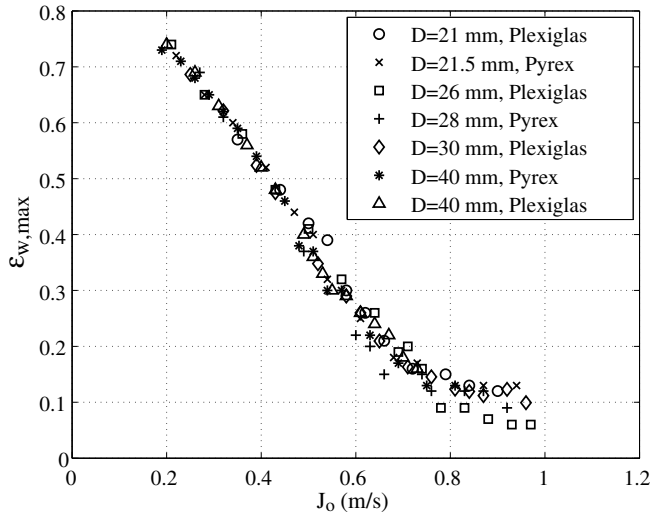

Fig. 14. Water input ratio corresponding to R_{max} as a function of the oil input ratio for all the pipe configurations tackled in the study.

The two models provide very close pressure drop predictions with small differences being observed only for $J_o = 0.64$ and 0.93 m/s, where the Brauner theory gives somewhat steeper curves. As expected the experimental points depart from the annular flow models as soon as a wavy stratified regime is established; this corresponds to $\varepsilon_w \approx 0.74$ for $J_o = 0.21$, $\varepsilon_w \approx 0.25$ for $J_o = 0.64$ and $\varepsilon_w \approx 0.05$ for $J_o = 0.93$. For $J_o = 0.21$ m/s the two annular flow models and the experimental data match very well despite the experiments falling in the slug regime region between $\varepsilon_w = 0.87$ and 0.74. In the annular flow regime ($J_o = 0.64$ and 0.93 m/s) both models slightly overpredict the pressure drop. Discrepancies fall within the measurement uncertainty of R only for $\varepsilon_w > 0.43$ in the $J_o = 0.64$ m/s case ($U_R(J_o = 0.64) \approx 4\%$) and for $\varepsilon_w > 0.34$ in the $J_o = 0.93$ m/s case ($U_R(J_o = 0.93) \approx 3\%$). This

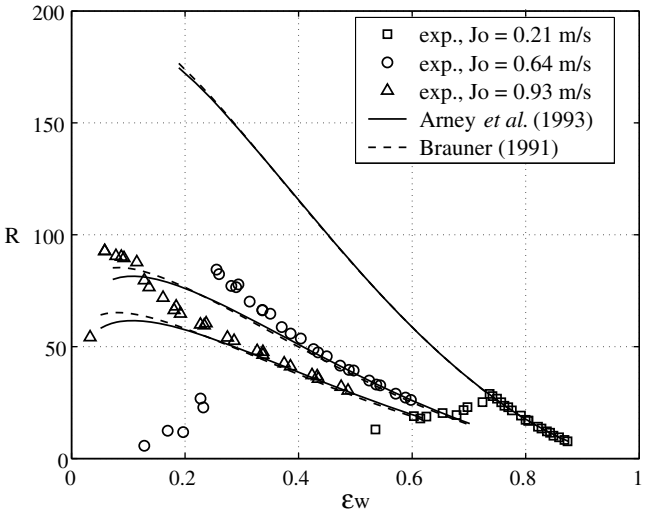

Fig. 15. Pressure drop reduction factor as a function of the water input ratio. Symbols indicate experimental points for $J_o = 0.21, 0.64, 0.93$ m/s in the $D = 26$ mm Plexiglas pipe; solid lines represent the Arney's model prediction, dashed lines display results from the model by Brauner (1991) for the same J_o as the experiments and $0.05 < J_w < 1.5$ m/s. The two curves representing the models are superimposed for a wide range of ε_w.

corresponds in both cases to $J_w > 0.48$, in the perfect annular regime (see Fig. 9).

Within this perfect annular regime region experimental results are well represented by both models, however discrepancies between the models exceed the measurement uncertainty in the wavy annular regime. As long as the flow regimes occurring do not involve contact of the oil to the wall, the general trend of the experimental data is followed by the models (5) and (12).

4.5. Conditions for annular/stratified transition

It is known (Arney et al., 1993) that in the core annular flow regime when the oil flow rate is held constant, the water flow rate which minimizes the pressure gradient is very near the one that leads to transition to the stratified regime, provided that such a transition will indeed occur. The identification of the boundary between the two flow patterns is required in order to determine the regions with operational conditions that are suitable for applications. In the following discussion, where the conditions for annular/stratified transition are sought, we consider a situation where a transition from annular to stratified flow can take place, namely with the oil superficial velocity below the critical value ($J_o < \widehat{J}_o$) and the pipe diameter large enough for the stratified regime to be sustained.

All of our measurements indicate that the water input ratio corresponding to the maximum reduction factor for a given oil flow rate is only weakly dependent on the pipe diameter. This is displayed in Fig. 14 and is even more evident for $J_o < \widehat{J}_o$, where $\varepsilon_{w,max}$ equals the water input ratio in transitional conditions $\varepsilon_{w,t}$. The water input ratio for which the annular/stratified transition takes place depends on the oil superficial velocity, on the physical properties of the fluids, but not on D:

$$\varepsilon_{w,t} = \varepsilon_{w,t}(\rho_o, \rho_w, \mu_o, \mu_w, \sigma, J_o) \tag{13}$$

The dependence of any parameter on the physical properties of the liquids cannot be negated because they are not varied in the present work.

Another result of the present experimental investigation is that the homogeneous model Froude number corresponding to the peak reduction factor appears to be independent of the oil superficial velocity when measured in a single horizontal pipe. The homogeneous model Froude number is defined as

$$Fr \equiv \frac{\rho_{ow} J_{ow}^2}{\Delta\rho\ gD} \tag{14}$$

where $\Delta\rho \equiv |\rho_w - \rho_o|$ and the mixture density is given by

$$\rho_{ow} \equiv \rho_o(1 - \varepsilon_w) + \rho_w \varepsilon_w \tag{15}$$

An example of this behavior is displayed in Fig. 16 where the normalized pressure drop $R^* = R/R_{max}$ measured in the $D = 26$-mm Plexiglas pipe is plotted against Fr for different oil superficial velocities. As mentioned above, the maximum reduction factor for a given oil superficial velocity ($J_o < \widehat{J}_o$) corresponds to the reduction factor in conditions very near to the annular/stratified transition, therefore the transition occurs at a Froude number Fr_t depending on the pipe diameter, but not on the oil superficial velocity:

$$Fr_t = Fr_t(\rho_o, \rho_w, \mu_o, \mu_w, \sigma, D) \tag{16}$$

When a equivalent velocity ω is defined as

$$\omega \equiv \sqrt{\frac{\rho_{ow} J_{ow}^2}{\Delta\rho}} \tag{17}$$

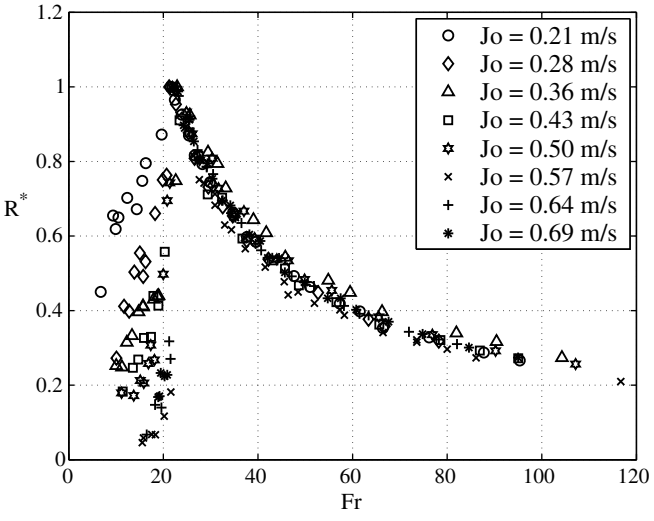

Fig. 16. Normalized pressure drop $R^* = R/R_{max}$ measured in the $D = 26$ mm Plexiglas pipe for different oil superficial velocities, $J_o < \widehat{J}_o$.

it can be concluded from Eqs. (13) and (16) that *its value across the annular/stratified transition* ω_t depends only on the properties of the two fluids.

Fig. 17 displays the equivalent velocity in transitional conditions as a function of the Re_A Reynolds number for all the configurations investigated and $J_o < \widehat{J}_o$. For the fluids and the range of pipe diameters of the present experiments, $\omega_t = 2.3$ m/s. The annular flow criterion $\omega > \omega_t$ in terms of the water and the oil superficial velocities writes

$$J_w > -\frac{J_o(\rho_o + \rho_w) - \sqrt{(\rho_o - \rho_w)\left[(\rho_o - \rho_w)J_o^2 - 4\omega_t^2\rho_w\right]}}{2\rho_w} \tag{18}$$

Condition (18) is shown as a dashed line in the flow pattern maps, Figs. 9 and 10.

Fig. 18 is a (J_o, J_w) map where Eq. (18) is compared to the present experimental results, to transitional boundaries obtained experimentally by other authors under similar conditions (Bannwart et al., 2004) and to the zero real characteristics boundary for a non dimensional wave number $\widetilde{k} = kD = 1$ given by a linear stability analysis of liquid-liquid systems (Brauner and Maron, 1992b). Experiments by Bannwart et al. were carried out in a $D = 28.4$-mm and for $\mu_o = 488$ Pa s, $\rho_o = 925.5$ kg/m^3, $\sigma = 29 \times 10^{-3}$ N/m.

Two conditions proposed by Bannwart (2001) and defining limits for the stability of the annular flow and for the existence of the stratified pattern, are also shown in the same Fig. 18. The first condition comes from Joseph et al. (1984) where the hydrodynamic stability theory is used for concluding that under a selected set of governing parameters like the equal density of the two phases, the annular flow is stable only when the viscous fluid occupies most of the cross section:

$$(1 - H_w) > \frac{1}{2} \tag{19}$$

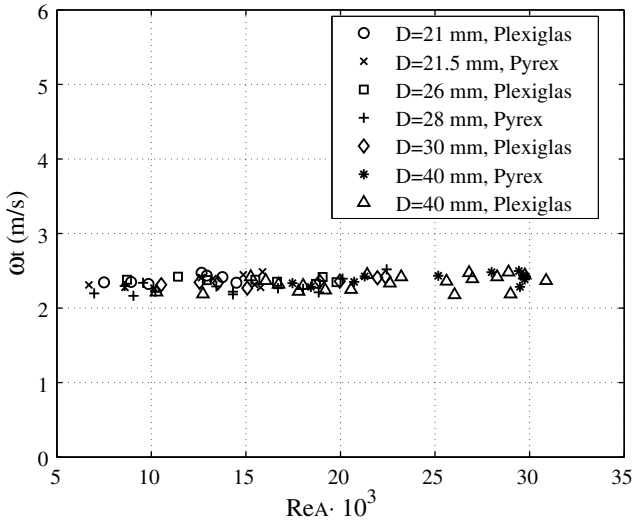

Fig. 17. Equivalent velocity ω in annular/stratified transition as a function of the Arney formulation of the Reynolds number, Eq. (10).

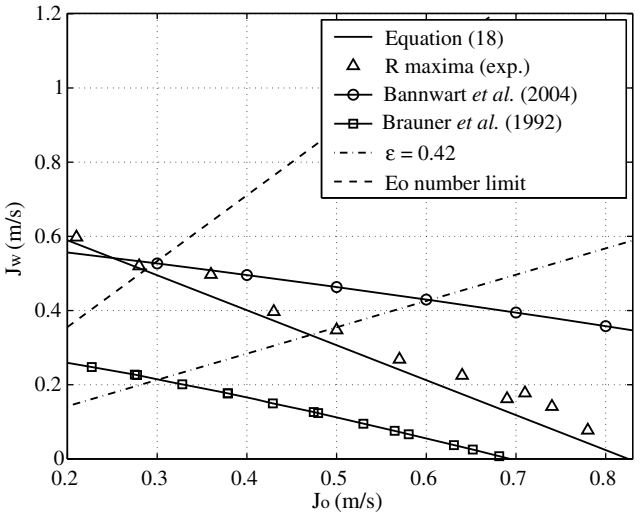

Fig. 18. Flow map for the 26-mm Plexiglas pipe: the solid line represent the equivalent velocity condition $\omega = \omega_t$ in the form of Eq. (18); triangles indicate measured reduction factor maxima. The annular/stratified limit from the experiments by Bannwart et al. (2004), the linear stability theory results by Brauner and Maron (1992b) and the criteria proposed by Bannwart (2001) are displayed for comparison purposes.

Eq. (19), together with the requirement that the thicker fluid has to be located at the core, which is always true in the present experiments, has been later re-interpreted (Bannwart, 2001) as a set of more general necessary criteria for the existence of core annular flow. Using the empirical formula (7) for reducing Eq. (19) to the measured variables gives $\varepsilon_w < 0.42$. The $\varepsilon_w = 0.42$ line displayed in Fig. 18 represents an upper limit above which core annular flow should not occur.

The second condition formulated by Bannwart (2001) indicates that occurrence of core flow in a pipe is possible when:

$$\frac{\pi\Delta\rho g D^2}{4\sigma}(1 - H_w) < 8 \tag{20}$$

Eq. (20) sets a limit to the Eötvös number: in gravity dominated two-phase systems the flow will undergo a transition to the stratified regime. The $Eo(1 - H_w) = 4/\pi$ line displayed in Fig. 18 for the present experiments in the 26-mm pipe represents a lower limit below which annular flow should not be sustained. Conditions (19) and (20) taken together exclude the existence of annular flow for $Eo \equiv \Delta\rho g D^2/8\sigma > 4/\pi$.

In contrast to condition (20), experimental results reveal that while increasing the oil superficial velocity, the stratified configuration is stable over a smaller J_w interval. Provided the annular flow can be sustained, it is stabilized by a higher mixture velocity and the annular/stratified boundary has a negative slope.

5. Conclusions

Water continuous oil–water flow is experimentally studied in seven different pipes of Plexiglas and Pyrex with diameter between 21 to 40 mm. The influence is discussed

of the inlet mixer shape, the pipe material and its history on the flow features. The pressure drop behavior is evaluated in terms of the oil–water interface shape and its modifications caused by variations of the flow rates. Results in perfect annular flow are shown to compare well with two widely used fully developed flow models from the literature. Detailed flow pattern maps for the 26- and 40-mm pipes are displayed in the article: the locus of points with peak reduction factor is very near the transition between the annular and stratified flow regimes.

An empirical law for the location of the annular/stratified transitional boundary is proposed which correctly predicts the boundary in a (J_o, J_w) map. Central to the criterion formulated is the idea that the momentum of the mixture has a stabilizing effect on the annular flow. The minimum homogeneous model momentum $\rho_{ow} J_{ow}^2$ transported in annular flow does depend upon the physical properties of the fluids but appears to be largely independent of the pipe diameter. The use of the suggested condition in applications is viable, requiring only a preliminary test to be performed with the same fluid pair. This ensures an accurate indication of the most suitable combinations of flow rates for water lubricated transportation of a highly viscous liquid.

Acknowledgments

The authors thank prof. M. Collins of the Brunel University for his careful proof-reading of the manuscript. The authors also thank prof. P. K. Das of the Indian Institute of Technology, Kharagpur, for the provision of the flow pattern map constructed experimentally and recently published (Chakrabarti et al., 2007). The map was not used here because of the too large difference in physical properties of the oil.

Financial support for this research was provided by the Italian MUR – Ministero Università e Ricerca.

References

Angeli, P., Hewitt, G.F., 1998. Pressure gradient in horizontal liquid–liquid flows. Int. J. Multiphase Flow 24, 1183–1203.

Angeli, P., Hewitt, G.F., 2000. Flow structure in horizontal oil–water flow. Int. J. Multiphase Flow 26, 1117–1140.

Arney, M.S., Bai, R., Guevara, E., Joseph, D.D., Liu, K., 1993. Friction factor and holdup studies for lubricated pipelining - I experiments and correlations. Int. J. Multiphase Flow 19, 1061–1076.

Bannwart, A.C., 2001. Modeling aspects of oil–water core-annular flows. J. Pet. Sci. Eng. 32, 127–143.

Bannwart, A.C., Rodriguez, O.M.H., deCarvalho, C.H.M., Wang, I.S., Vara, R.M.O., 2004. Flow patterns in heavy crude oil–water flow. ASME J. Energy Resources Technol. 126, 185–189.

Brauner, N., 1991. Two-phase liquid–liquid annular flow. Int. J. Multiphase Flow 17, 59–76.

Brauner, N., 2001. The prediction of dispersed flows boundaries in liquid–liquid and gas–liquid systems. Int. J. Multiphase Flow 27, 886–910.

Brauner, N., Maron, D.M., 1992a. Flow pattern transitions in two-phase liquid–liquid flow in horizontal tubes. Int. J. Multiphase Flow 18, 123–140.

Brauner, N., Maron, D.M., 1992b. Stability analysis of stratified liquid–liquid flow. Int. J. Multiphase Flow 18, 103–121.

Chakrabarti, D.P., Das, G., Das, P.K., 2007. Identification of stratified liquid–liquid flow through horizontal pipes by a non-intrusive optical probe. Chem. Eng. Sci. 62, 1861–1876.

dos Santos, R.G., Mohamed, R.S., Bannwart, A.C., Loh, W., 2006. Contact angle measurements and wetting behavior of inner surfaces of pipelines exposed to heavy crude oil and water. J. Petrol. Sci. Eng. 51, 9–16.

Joesph, D.D., Bai, R., Mata, C., Sury, K., Grant, C., 1999. Self-lubricated transport of bitumen froth. J. Fluid Mech. 386, 127–148.

Joseph, D.D., Bai, R., Chen, K.P., Renardy, Y.Y., 1997. Core-annular flows. Annu. Rev. Fluid Mech. 29, 65–90.

Joseph, D.D., Renardy, M., Renardy, Y., 1984. Instability of the flow of two immiscible liquids with different viscosities in a pipe. J. Fluid Mech. 141, 309–317.

Joseph, D.D., Renardy, Y.Y., 1993. Fundamentals of Two-Fluid Dynamics. Part II: Lubricated Transport, Drops and Miscible Liquids. Springer-Verlag, Berlin.

Lovick, J., Angeli, P., 2004. Experimental studies on the dual continuous flow pattern in oil–water flows. Int. J. Multiphase Flow 30, 139–157.

Marchesi, R., Mello, M.S., Mengozzi, S., 2004. Measurement uncertainty applied to the main parameters in oil–water flows and related critical transitions. In: International Symposium on Two-Phase Flow Modeling and Experimentation, vol. 4. ETS, Pisa, pp. 2615–2620.

Oliemans, R.V.A., Ooms, G., 1986. Core-annular flow of oil and water through a pipeline. In: Hewitt, G.F., Delhaye, J.M., Zuber, N. (Eds.), Multiphase Science and Technology, vol. 2. Hemisphere Publishing Corporation, Washington, DC, pp. 427–477.

Oliemans, R.V.A., Ooms, G., Wu, H.L., Duijvestijn, A., 1987. Core-annular oil/water flow: turbulent-lubricating-film model and measurements in a 5 cm pipe loop. Int. J. Multiphase Flow 13, 23–31.

Ooms, G., 1972. The hydrodynamic stability of core-annular flow of two ideal liquids. Appl. Sci. Res. 26, 147–158.

Ooms, G., Beckers, H.L., 1972. The flow of a rigid core surrounded by an annular liquid layer through a horizontal tube. Appl. Sci. Res. 26, 321–334.

Ooms, G., Poesio, P., 2003. Stationary core-annular flow through a horizontal pipe. Phys. Rev. E 68, 066301.

Russel, T.W.F., Charles, M.E., 1959. The effect of the less viscous liquid in the laminar flow of wo immiscible liquids. Can. J. Chem. Eng. 37, 18–24.

Ullmann, A., Brauner, N., 2004. Closure relations for the shear stress in two-fluid models for core-annular flow. Multiphase Sci. Technol. 16, 355–387.